

# Mass and energy balance calculations for an artificial ice reservoir (Icestupa)

Suryanarayanan Balasubramanian<sup>1,\*</sup>, Martin Hoelzle<sup>1</sup>, Michael Lehning<sup>2</sup>,  
Sonam Wangchuk<sup>3</sup>, Johannes Oerlemans<sup>4</sup> and Felix Keller<sup>5</sup>

<sup>1</sup>University of Fribourg, Fribourg, Switzerland

<sup>2</sup>WSL Institute for Snow and Avalanche Research, Davos, Switzerland

<sup>3</sup>Himalayan Institute of Alternatives Ladakh, Leh, India

<sup>4</sup>Institute for Marine and Atmospheric Research, Utrecht University, Utrecht, The Netherlands

<sup>5</sup>Academia Engiadina, Samedan, Switzerland

Correspondence\*:

Suryanarayanan Balasubramanian

suryanarayanan.balasubramanian@unifr.ch

## ABSTRACT

Artificial Ice Reservoirs (AIR) have been successful in storing water during winter and releasing the water during spring and summer. This has made them a reliable fresh water resource for irrigation in dry environments. Several AIRs have been built but studies of their water storage capacity and efficiency are scarce. This study attempts to model a cone-shaped AIR popularly called Icestupa. Important processes involved in the development and temporal evolution of an Icestupa are calculated by a physically-based model using equations governing the heat transfer, vapour diffusion and water transport of a phase changing water mass. These processes were quantified by using meteorological data in conjunction with fountain spray information (mass input of an Icestupa) to estimate the quantity of frozen, melted, evaporated and drained water at a location called 'Eispalast' in the Schwarzsee region in the Canton of Fribourg, Switzerland. At this measurement site, an Icestupa was built for model validation purposes. The model was further tested by performing sensitivity and uncertainty study showing that the most sensitive parameters are the temperature threshold used to determine precipitation phase and the ice emissivity. Model calculations estimate that the Schwarzsee Icestupa only stored about 8% of the total water sprayed as ice. In addition, we found that reducing nozzle diameter of the fountain to 3 mm increases the storage efficiency up to 93% without compromising on the storage duration.

**Keywords:** iclestupa, mass balance, water storage, climate change adaptation, geoengineering

## 1 INTRODUCTION

Seasonal snow cover, glaciers and permafrost are expected to change their water storage capacity due to climate change with major consequences for downriver water supply (Immerzeel et al., 2019). The challenges brought about by these changes are especially important for dry mountain environments such as in Central Asia or Andes, which directly rely on the seasonal meltwater for their farming and drinking needs (Hoelzle et al., 2019; Apel et al., 2018; Buytaert et al., 2017; Chen et al., 2016; Unger-Shayesteh



**Figure 1.** Icestupa in Ladakh, India on March 2017 was 24 m tall and contained around 3.7 million litres of water. Picture Credits: Lobzang Dadul

et al., 2013). Some villages in Ladakh, India have already been forced to relocate due to glacial retreat and the corresponding loss of their main fresh water resources (Grossman, 2015).

Artificial Ice Reservoirs (AIR) have been considered to be a feasible way to adapt to these changes (Hock et al., 2019; Nüsser et al., 2019b). An artificial ice reservoir is a human-made ice structure typically constructed during the cold winter months and designed to slowly release freshwater during the warm and dry spring and summer months. The main purpose of AIR is irrigation. Therefore, AIRs are designed to store water in the form of ice as long into the summer as possible. The energy required to construct an AIR is usually derived from the gravitational head of the source water body. Some are constructed horizontally by freezing water using a series of checkdams and others are built vertically by spraying water through fountain systems (Nüsser et al., 2019a). The latter are colloquially referred to as Icestupas and are the subject of this study.

Since their invention in 2013 (Wangchuk, 2014), Icestupas have gained widespread publicity in the region of Ladakh, Northern India since they require very little infrastructure, skills and energy to be constructed in comparison to other water storage technologies. Compared to other AIR geometries, the conical shape of the Icestupas (Fig. 1) have been proven as an optimal geometry, which can be built at lower altitudes and last much longer into the summer than ice structures with other geometries (Wangchuk, 2014).

If AIR are to become a viable water resource management tool, it is crucial to be able to propose suitable construction sites, and to identify and optimize water losses. However, to date, no reliable estimates exist about the amount of sprayed water that is necessary to create them and the meltwater they provide (Nüsser et al., 2019a). Moreover, such estimates depend heavily on the prevailing weather conditions and water availability at the construction site. Rough estimates of Icestupa meltwater in Ladakh suggest that the water loss during the construction process is considerable (see Appendix 8.1). A complete set of measurements of the water and energy balance are urgently required to understand the cause of the water losses better and increase the construction efficiency.

In this paper, we aim to develop a physically-based model of a vertical AIR (or Icestupa) that can quantify their storage efficiency using existing weather and water usage information. Mass and energy balance equations were used to estimate the quantity of water frozen, melted, evaporated and wasted. Sensitivity

and uncertainty analysis were performed to identify the most sensitive parameters and the variance caused by them. For validation, we created an Icestupa at a well accessible site (called Eispalast) near Schwarzsee in the Canton of Fribourg, Switzerland, allowing easy maintenance and control of the measurements. Due to the low altitude of the site with relatively high winter temperatures only a small Icestupa could be established during winter 2018/19 for providing us with model validation data. Our model and validation experiments provide first steps towards an evaluation of the effectiveness of a vertical AIR for irrigation and finally we outline some preliminary guidelines for consideration when a construction of an Icestupa for water storage is envisaged.

## 2 STUDY SITE

The 'Eispalast' site in the Schwarzsee region lies on 967 m a.s.l. In the winter (Oct-Mar), the mean daily maximum and minimum of the air temperatures vary between 14 to  $-4^{\circ}\text{C}$ . Clear skies are rare averaging around 7 days and precipitation amounts average at 155 mm per month during winter (Meteoblue, 2020). The site was also situated adjacent to a stream resulting in high humidity values across the study period. Within the 'Eispalast' site, an enclosure of 1.8 m in radius was constructed for the experiment. An automatic weather station (AWS) was set in place adjacent to the wooden boundary as shown in Fig. 2. The fountain used for spraying water had a nozzle diameter of 5 mm and a height of 1.35 m, and was placed in the centre of the wooden enclosure. The water was transferred from a spring water source at 1267 m a.s.l. by a pipeline and flowed via a flowmeter and an air escape valve to the nozzle, where it was sprinkled with a spray radius of around 1.7 m. The air escape valve was installed to avoid errors in the flow measurements due to air bubbles. In addition, a webcam guaranteed a continuous survey of the site during the construction of the Icestupa.

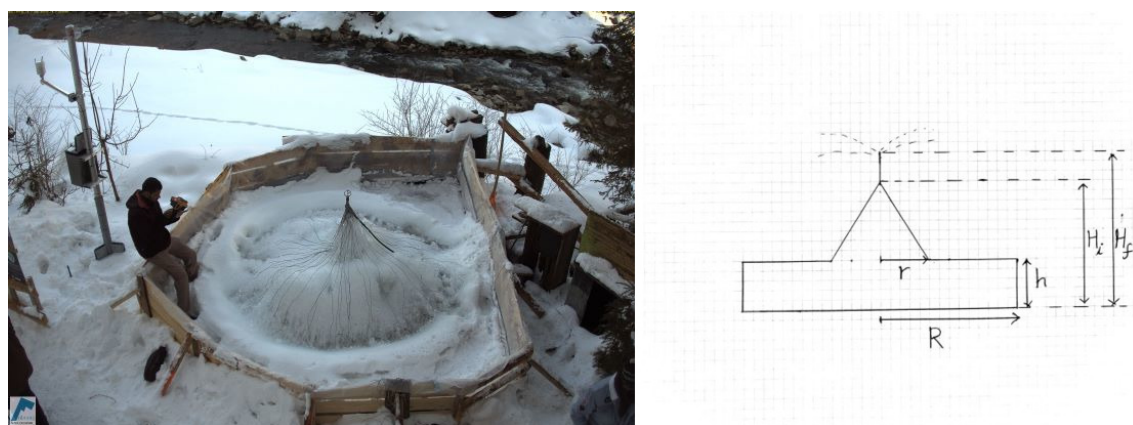


**Figure 2.** The ice structure during the first validation measurement as seen on the webcam image of 14<sup>th</sup> Feb. The corresponding cross section of the Schwarzsee ice structure with the field estimates of  $r$ ,  $R$ ,  $h$ ,  $H_i$ ,  $H_f$  used to determine the Icestupa volume is shown on the right.

### 2.1 Construction

From 30<sup>th</sup> January to 18<sup>th</sup> March 2019 the Icestupa was constructed through the fountain spray, which was manually switched on if measured air temperature was below  $-5^{\circ}\text{C}$  after sunset and was switched off as soon as the ice was exposed to daylight or temperatures were above  $0^{\circ}\text{C}$ . The water spray of the fountain was initially adjusted so that most of the water droplets land within the wooden boundary zone. The ice formation was guided by adding a metal framework at the ice structure base after the first night of

operation. Several cotton threads were tied between the ice structure base and fountain pole for accelerating and further guiding the ice formation process.

## 2.2 Measurements and Data

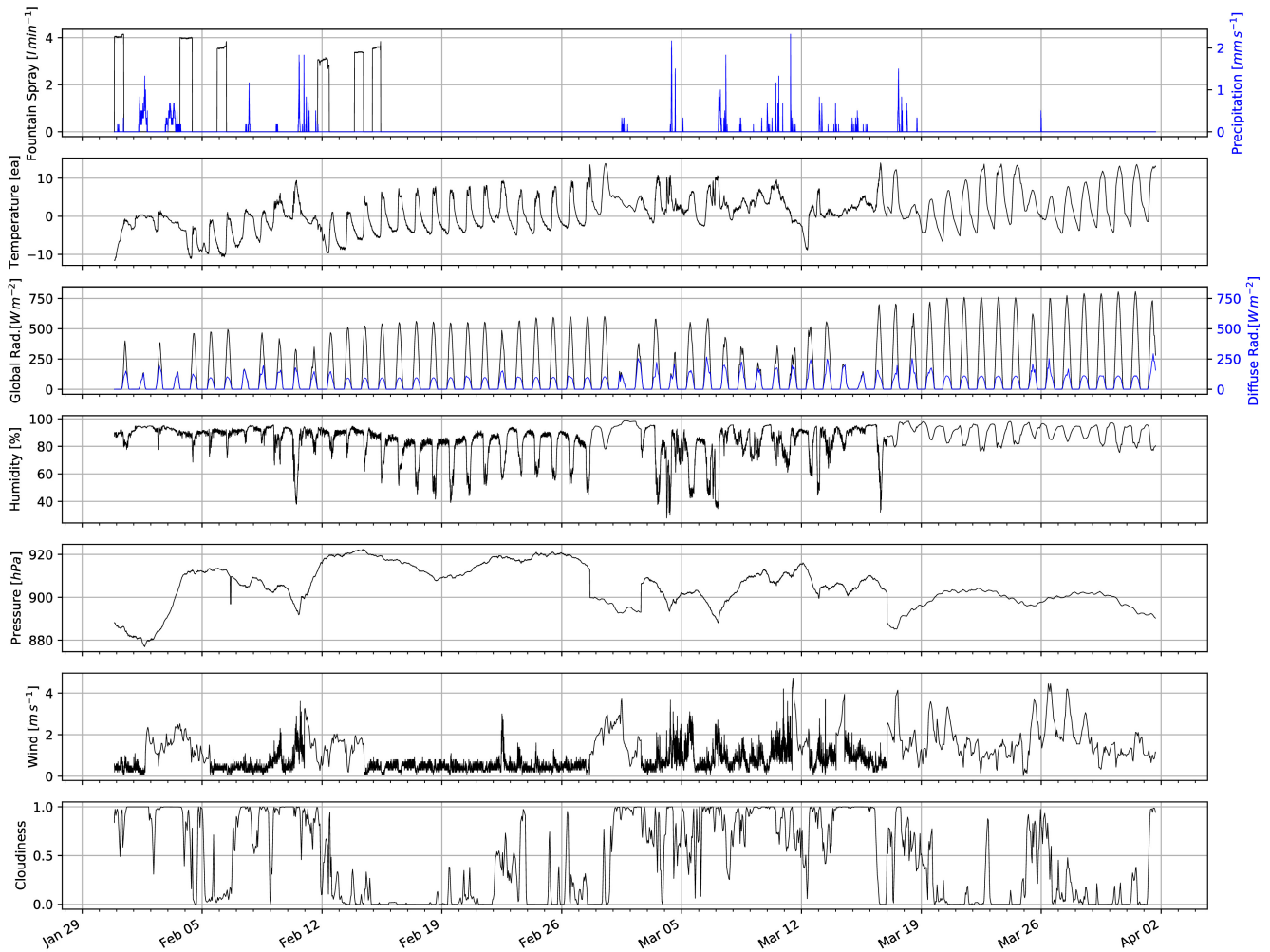


**Figure 3.** Measurements at the AWS of Schwarzsee were used as main model input data in 5 minute frequency. Plaffeien AWS provided the precipitation data. Cloudiness and incoming shortwave radiation were obtained from the ERA5 reanalysis dataset.

The Schwarzsee AWS was located at 967 *m* a.s.l. It was in operation from 30<sup>th</sup> January to 18<sup>th</sup> March 2019. Measurements comprise air temperature, relative humidity, water flow, wind speed and direction. All these measurements were stored as 5 minute means. Precipitation data was derived from the Plaffeien AWS (IDAWEB, 2019) located 8.8 km away from the measurement site at an altitude of 1042 *m* a.s.l. In order to acquire cloudiness and incoming shortwave radiation data, we used the ERA5 reanalysis dataset at Schwarzsee (Copernicus Climate Change Service (C3S), 2017). The hourly ERA5 data and the 10 minute Plaffeien AWS data were linearly interpolated to the 5 minute data frequency of the Schwarzsee AWS.

Due to a power failure, all data from the Schwarzsee AWS was lost between 27<sup>th</sup> February 15:20 to 2<sup>nd</sup> March 15:00. Consequently, the amount of missing data in the dataset was around 6.7%. During heavy snowfall events, the ultrasonic wind sensor was blocked and recorded zero values. These data gaps and errors were filled with the Plaffeien AWS precipitation and ERA5 reanalysis dataset. ERA5 air temperature

was found to be highly correlated ( $r^2 = 0.85$ ) with the Schwarzsee dataset but the corresponding wind speed values were poorly correlated ( $r^2 = 0.18$ ). However, in a second step, we further extended the dataset beyond 18<sup>th</sup> March 2019 (Fig. 3) to enable the model to completely melt the Icestupa.

### 2.2.1 Field Measurements for validation

Estimates of the ice volumes were obtained by two manual measurements of the ice structure dimensions. The first corresponds to the end of the freezing period on 14<sup>th</sup> February 16:00 (only one more fountain run was possible after this date). The second corresponds to the end of the melting process on 10<sup>th</sup> March 18:00. The field validations are shown by green line segments in Fig. 8.

On 14<sup>th</sup> February the ice volume was calculated using a simplistic cross section of the structure as shown in Fig. 2. We used the following field estimates of  $r, R, h, H_i, H_f$  (see Fig. 2 for the different geometry components) to determine the maximum and minimum volumes:

$$0.55 \leq r \leq 1m ; 1.1 \leq R \leq 1.2m ; 0.1 \leq h \leq 0.2m ; 0.6 \leq H_i \leq 0.8m ; 1.3 \leq H_f \leq 1.4m \quad (1)$$

The second validation point was considered to be on March 10<sup>th</sup> 18:00. Based on the webcam imagery and manual measurement, a thin layer of ice with an observed thickness between 0.01 to 0.06 m could be quantified. This results in an ice volume estimate for the first validation date on 14<sup>th</sup> February 2019 to be  $0.857 \pm 0.186 m^3$  and for the second validation date on 11<sup>th</sup> March 2019 to be  $0.13 \pm 0.09 m^3$ .

In reality, the Schwarzsee ice structure was more cylindrical until a height of 0.2 m and conical afterwards until a height of 0.6 m with a radius of 1.18 m. However, we assume a conical shape of this ice structure in order to apply the modelling strategy described below.

## 3 MODEL SETUP

The model (implemented in python) consists of three parts calculating a) the geometric evolution of the Icestupa, b) the energy balance and c) the mass balance as shown schematically in Fig. 4. A bulk energy and mass balance model is used to calculate the amounts of ice, liquid water, water vapour and drained water of the Icestupa every 5 minutes. The equations used henceforth display model time step superscript only if it is different from the current time step.

### 3.1 Icestupa geometric evolution

Radius  $r_{ice}$  and height  $h_{ice}$  define the dimensions of the Icestupa assuming its geometry to be a cone as shown in Fig. 5. The surface area  $A$  and volume  $V$  exposed to the atmosphere are:

$$A = \pi \cdot r_{ice} \cdot \sqrt{r_{ice}^2 + h_{ice}^2} \quad (2)$$

$$V = \pi/3 \cdot r_{ice}^2 \cdot h_{ice} \quad (3)$$

With the mass of the Icestupa  $M_{ice}$ , its current volume can also be expressed as:

$$V = M_{ice} / \rho_{ice} \quad (4)$$



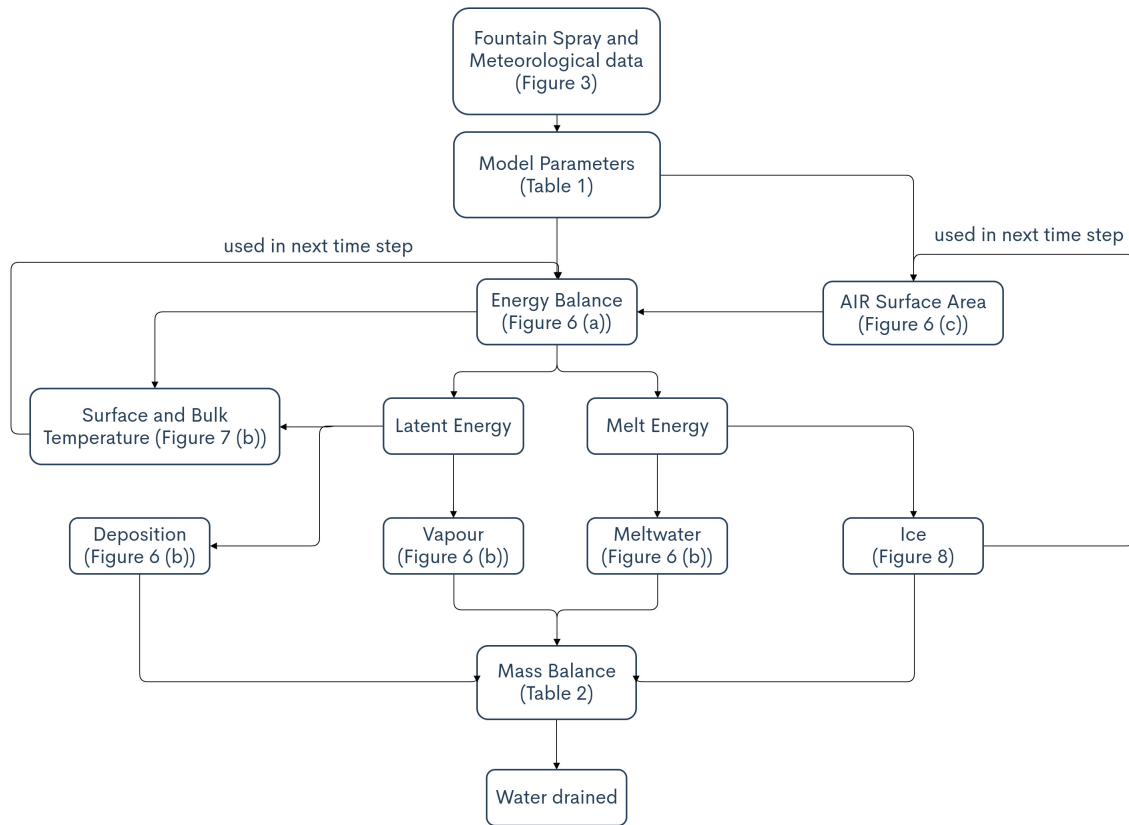


**Figure 4.** Model schematic showing the algorithm used in the model at every time step. Further details about these variables can be found in the associated tables and figures.

where  $\rho_{ice}$  is the density of ice ( $917 \text{ kg m}^{-3}$ ). The model of the Icestupa is initialised with a thickness of  $\Delta x$  (defined in 3.2) and a circular area of radius  $r_F$ . The constant  $r_F$  represents the mean spray radius of the fountain derived by modelling the projectile motion of water droplets as shown in appendix section 8.2. During subsequent time steps, the dimensions of the Icestupa evolve assuming a uniform ice formation and decay across its surface area with an invariant slope  $s_{cone} = \frac{h_{ice}}{r_{ice}}$  as shown in Fig. 5. During these time steps, the volume is parameterised using Eqn. 3 as:

$$V = \pi/3 \cdot r_{ice}^3 \cdot s_{cone} \quad (5)$$

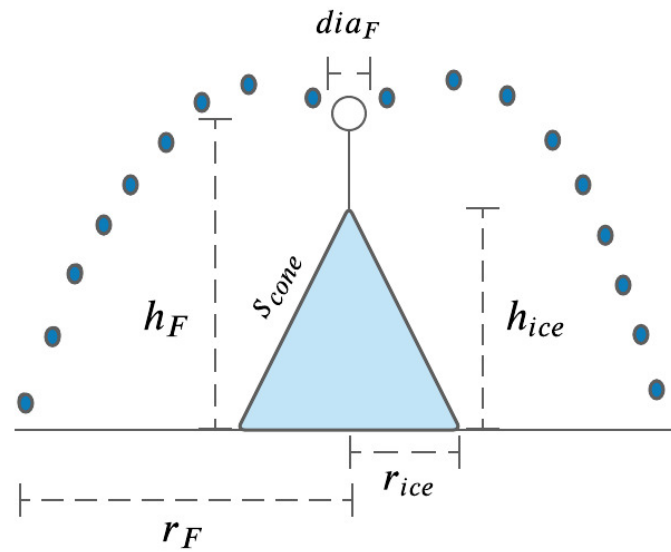


**Figure 5.** Shape and fountain parameters of the Schwarzsee Icestupa.  $r_{ice}$  is the radius,  $h_{ice}$  is the height and  $s_{cone}$  is the slope of the ice cone.  $r_F$  is the spray radius,  $h_F$  is the height and  $dia_F$  is the nozzle diameter of the fountain.

However, the Icestupa cannot outgrow the maximum range of the water droplets ( $(r_{ice})_{max} = r_F$ ). Combining equations 3, 4 and 5, the geometric evolution of the Icestupa at each time step  $i$  can be determined by considering the following rules:

$$(r_{ice}, h_{ice}) = \begin{cases} (r_F, \Delta x) & \text{if } i = 0 \\ (r_{ice}^{i-1}, \frac{3 \cdot M_{ice}}{\pi \cdot \rho_{ice} \cdot (r_{ice}^{i-1})^2}) & \text{if } r_{ice}^{i-1} \geq r_F \text{ and } \Delta M_{ice} > 0 \text{ where } \Delta M_{ice} = M_{ice}^{i-1} - M_{ice}^{i-2} \\ (\frac{3 \cdot M_{ice}}{\pi \cdot \rho_{ice} \cdot s_{cone}})^{1/3} \cdot (1, s_{cone}) & \text{otherwise} \end{cases} \quad (6)$$

### 3.2 Energy Balance

The energy balance equation for the Icestupa is formulated as follows:

$$q_{net} = q_{SW} + q_{LW} + q_L + q_S + q_F + q_G \quad (7)$$

where  $q_{net}$  is the net energy flux in [ $W m^{-2}$ ];  $q_{SW}$  is the net shortwave radiation;  $q_{LW}$  is the net longwave radiation;  $q_L$  and  $q_S$  are the turbulent latent and sensible heat fluxes.  $q_F$  represents the heat exchange created due to the additional water and ice boundary present during fountain on time steps.  $q_G$  represents ground heat flux between Icestupa surface and Icestupa interior. Energy transferred in the direction of the ice surface is always denoted as positive and away as negative. Also, all temperature variables are assigned in units of [ $^{\circ}C$ ].

Equation 7 is usually referred to as the energy budget for “the surface”, but practically it must apply to a surface layer of ice with a finite thickness  $\Delta x$ . The energy flux acts upon the Icestupa surface layer

which has an upper and a lower boundary defined by the atmosphere and the ice body of the Icestupa, respectively. The parameter selection for  $\Delta x$  is based on the following two arguments: (a) the ice thickness  $\Delta x$  should be small enough to represent the daily surface temperature variations with its high amplitude. (b)  $\Delta x$  requires to be large enough for these temperature variations to not reach the bottom of the surface layer. Therefore, we introduced a 5 mm thick ice surface layer, over which the energy balance is calculated. A sensitivity analysis was later performed to understand the influence of this factor. Here, we define the surface temperature  $T_{ice}$  to be the modelled average temperature of the Icestupa surface layer and the energy flux  $q_{net}$  is assumed to act uniformly across the Icestupa area  $A$ .

### 3.2.1 Net Shortwave Radiation $q_{SW}$

The net shortwave radiation  $q_{SW}$  is computed as follows:

$$q_{SW} = (1 - \alpha) \cdot (SW_{direct} \cdot f_{cone} + SW_{diffuse}) \quad (8)$$

where  $SW_{direct} = SW_{global} - SW_{diffuse}$  with the measured global and diffuse short wave radiation as  $SW_{global}$  and  $SW_{diffuse}$ , the modelled albedo as  $\alpha$  and with  $f_{cone}$  as the area fraction of the ice structure exposed to the direct shortwave radiation.

We model the albedo using a scheme described in Oerlemans and Knap (1998). The scheme records the decay of albedo with time after fresh snow is deposited on the surface.  $\delta t$  records the number of time steps after the last snowfall event. After snowfall, albedo changes over a time step,  $\delta t$ , as

$$\alpha = \alpha_{ice} + (\alpha_{snow} - \alpha_{ice}) \cdot e^{(-\delta t)/\tau} \quad (9)$$

where  $\alpha_{ice}$  is the bare ice albedo value and  $\tau$  is a decay rate, which determines how fast the albedo of the ageing snow reaches this value. The decay rate  $\tau$  is assumed to have a base value of 10 days similar to values obtained by Schmidt et al. (2017) for wet surfaces and its maximal value is set based on observations by Oerlemans and Knap (1998) as shown in Table 1. Furthermore, the albedo  $\alpha$  varies depending on the water source that formed the current Icestupa surface. Correspondingly, the albedo is reset to the value of bare ice albedo if the fountain is spraying water onto the current ice surface and to the value of fresh snow albedo if a snowfall event occurred. Snowfall events are assumed if the air temperature is below  $T_{rain} = 1^\circ C$ .

The area fraction  $f_{cone}$  of the ice structure exposed to the direct shortwave radiation depends on the shape considered. This factor is derived by calculating the area influenced by the vertical and horizontal components of the direct solar radiation. For a conical shape, half of the total curved surface is exposed to the vertical component of the direct shortwave radiation and the projected triangle of the curved surface is exposed to the horizontal component of the direct shortwave radiation. The solar elevation angle  $\theta_{sun}$  used is modelled using the parametrisation proposed by Woolf (1968). Accordingly,  $f_{cone}$  is determined as follows:

$$f_{cone} = \frac{(0.5 \cdot r_{ice} \cdot h_{ice}) \cdot \cos \theta_{sun} + (\pi \cdot r_{ice}^2 / 2) \cdot \sin \theta_{sun}}{\pi \cdot r_{ice} \cdot (r_{ice}^2 + h_{ice}^2)^{1/2}} \quad (10)$$

The measured diffuse shortwave radiation is assumed to impact the conical Icestupa surface uniformly.



### 3.2.2 Net Longwave Radiation $q_{LW}$

The net longwave radiation  $q_{LW}$ , for which there were no direct measurements available at Schwarzsee, is determined as follows:

$$q_{LW} = \sigma \cdot (\epsilon_a \cdot (T_a + 273.15)^4 - \epsilon_{ice} \cdot (T_{ice} + 273.15)^4) \quad (11)$$

where  $T_a$  represents the measured air temperature,  $T_{ice}$  is the modelled surface temperature, both temperatures are given in  $^{\circ}C$ ,  $\sigma = 5.67 \cdot 10^{-8}$  is the Stefan-Boltzmann constant,  $\epsilon_a$  denotes the atmospheric emissivity and  $\epsilon_{ice}$  is the corresponding emissivity value for the Icestupa surface (see Table 1).

For the calculation of the incoming longwave radiation, we approximate atmospheric emissivity  $\epsilon_a$  using the equation suggested by Brutsaert (1982), considering air temperature and vapor pressure (Eqn. 13). The vapor pressures over air and ice was obtained using the following formulation given in WMO (2018):

$$\begin{aligned} p_{v,a} &= 6.107 \cdot 10^{(7.5 \cdot T_a / (T_a + 237.3))} \\ p_{v,ice} &= (1.0016 + 3.15 \cdot 10^{-6} \cdot p_a - 0.074 \cdot p_a^{-1}) \cdot (6.112 \cdot e^{(22.46 \cdot T_{ice} / (T_{ice} + 272.62))}) \end{aligned} \quad (12)$$

where  $p_{v,a}$  denotes the saturation vapor pressure of air,  $p_{v,ice}$  denotes the saturation vapor pressure of ice and  $p_a$  is the measured air pressure in  $[hPa]$ . The expression defined in Brutsaert (1975) for clear skies (first term in equation 13) is extended with the correction for cloudy skies after Brutsaert (1982) as follows:

$$\epsilon_a = 1.24 \cdot \left( \frac{p_{v,a}}{(T_a + 273.15)} \right)^{1/7} \cdot (1 + 0.22 \cdot c^2) \quad (13)$$

with a cloudiness index  $c$ , ranging from 0 for clear skies to 1 for complete overcast skies, obtained from the ERA5 reanalysis data as shown in Fig. 3.

### 3.2.3 Turbulent sensible $q_S$ and latent $q_L$ heat fluxes

The turbulent sensible  $q_S$  and latent heat  $q_L$  fluxes are computed with the following expressions proposed by Garratt (1992):

$$q_S = c_a \cdot \rho_a \cdot p_a / p_{0,a} \cdot \frac{\kappa^2 \cdot v_a \cdot (T_a - T_{ice})}{\left( \ln \frac{h_{AWS}}{z_{ice}} \right)^2} \quad (14)$$

$$q_L = \begin{cases} 0.623 \cdot L_s \cdot \rho_a / p_{0,a} \cdot \frac{\kappa^2 \cdot v_a (p_{v,a} - p_{v,ice})}{\left( \ln \frac{h_{AWS}}{z_{ice}} \right)^2} & \text{if } \Delta M_F = 0 \\ 0 & \text{if } \Delta M_F > 0 \text{ where } \Delta M_F = M_F^i - M_F^{i-1} \end{cases} \quad (15)$$

where  $h_{AWS}$  is the measurement height above the ground surface of the AWS (in  $m$ ),  $v_a$  is the wind speed in  $[m \cdot s^{-1}]$  and  $M_F$  denotes fountain water spray mass in  $[kg]$ .  $c_a$  is the specific heat of air at constant pressure ( $1010 \text{ J } kg^{-1} K^{-1}$ ),  $\rho_a$  is the air density at standard sea level ( $1.29 \text{ kg } m^{-3}$ ),  $p_{0,a}$  is the air pressure at standard sea level ( $1013 \text{ hPa}$ ),  $\kappa$  is the von Karman constant (0.4),  $L_s$  is the heat of sublimation ( $2848 \text{ kJ } kg^{-1}$ ) and  $z_{ice}$  ( $1.7 \text{ mm}$ ) denotes the roughness length of ice (momentum and scalar).

### 3.2.4 Fountain water heat flux $q_F$

The total energy flux is further influenced through the heat flux caused by the water that was additionally added to the surface of the Icestupa during the time the fountain was running. We take this interaction between the fountain water and the ice surface into account by assuming that the ice surface temperature stays constantly at  $0^\circ\text{C}$  during time steps when the fountain is active. This process can be divided into two simultaneous steps: (a) the water temperature  $T_{water}$  is cooled to  $0^\circ\text{C}$  and (b) the ice surface temperature is warmed to  $0^\circ\text{C}$ . Process (a) transfers hereby the necessary energy for process (b) throughout the fountain runtime. We further assume that this process is instantaneous, i.e. the ice temperature is immediately set to  $0^\circ\text{C}$  within just one time step  $\Delta t$  when the fountain is switched on. Thus, the heat flux caused by the fountain water is calculated as follows:

$$q_F = \begin{cases} 0 & \text{if } \Delta M_F = 0 \\ \frac{\Delta M_F \cdot c_{water} \cdot T_{water}}{\Delta t \cdot A} + \frac{\rho_{ice} \cdot \Delta x \cdot c_{ice} \cdot T_{ice}}{\Delta t} & \text{if } \Delta M_F > 0 \end{cases} \quad (16)$$

with  $c_{ice}$  as the specific heat of ice.

### 3.2.5 Bulk Icestupa heat flux $q_G$

The bulk Icestupa heat flux  $q_G$  corresponds to the ground heat flux in normal soils and is caused by the temperature gradient between the surface layer and the ice body. It is expressed by using the heat conduction equation as follows:

$$q_G = k_{ice} \cdot (T_{bulk} - T_{ice}) / l_{ice} \quad (17)$$

where  $k_{ice}$  is the thermal conductivity of ice in  $[W m^{-1} K^{-1}]$ ,  $T_{bulk}$  is the mean temperature of the ice body within the Icestupa and  $l_{ice}$  is the average distance of any point in the surface to any other point in the ice body.  $T_{bulk}$  is initialised as  $0^\circ\text{C}$  and later determined from Eqn. 17 as follows:

$$T_{bulk} = T_{bulk}^{i-1} - (q_G \cdot A \cdot \Delta t) / (M_{ice} \cdot c_{ice}) \quad (18)$$

Since we assume a conical shape with  $r_{ice} > h_{ice}$ ,  $l_{ice}$  cannot be greater than  $2r_{ice}$  and also cannot be less than  $\Delta x$ . Therefore, the average distance from any point on the surface to any point inside is  $\Delta x \leq l_{ice} \leq r_{ice}$ . We calculate  $q_G$  here assuming  $l_{ice} = r_{ice}/2$ .

### 3.2.6 Surface temperature changes and melt energy $q_{melt}$

The available net energy  $q_{net}$  partly increases surface temperature, but also contributes to ice melt at the surface of the Icestupa.  $q_T$  denotes the energy used on changing the surface temperature  $T_{ice}$  and  $q_{melt}$  denotes the energy used to produce meltwater. So Eqn. 7 can be rewritten as:

$$q_{net} = q_{melt} + q_T \quad (19)$$

The temperature fluctuates based on 3 scenarios namely, (a) the energy flux is negative but cannot freeze all the fountain water output; (b) the energy flux is negative and can freeze all the fountain water output and (c) the fountain is inactive ( $\Delta M_F = 0$ ). Also, the latent heat always contributes to temperature fluctuations. Therefore, we express the rate of change of temperature as follows:

$$\frac{\Delta T}{\Delta t} = \begin{cases} -T_{ice}^{i-1}/\Delta t & \text{if } (q_{net} - q_L) < 0 \text{ and } \Delta M_F \geq -(q_{net} - q_L) \cdot A \cdot \Delta t / L_f \\ (\Delta M_F \cdot L_f) / (\rho_{ice} \cdot c_{ice} \cdot \Delta x \cdot A \cdot \Delta t) & \text{if } (q_{net} - q_L) < 0 \text{ and } \Delta M_F < -(q_{net} - q_L) \cdot A \cdot \Delta t / L_f \\ q_{net} / (\rho_{ice} \cdot c_{ice} \cdot \Delta x) & \text{if } \Delta M_F = 0 \end{cases} \quad (20)$$

Whenever the model predicts  $T_{ice}^{i+1} > 0^\circ C$ , then the surface temperature is set to  $0^\circ C$  in the corresponding time step and additional energy contributes to  $q_{melt}$ . Combining these requirements, we get:

$$(q_T, q_{melt}) = \begin{cases} (\rho_{ice} \cdot c_{ice} \cdot \Delta x \cdot \frac{\Delta T}{\Delta t}, q_{net} - q_L - \rho_{ice} \cdot c_{ice} \cdot \Delta x \cdot \frac{\Delta T}{\Delta t}) & \text{if } T_{ice}^{i+1} \leq 0 \text{ and } \Delta M_F > 0 \\ (\rho_{ice} \cdot c_{ice} \cdot \Delta x \cdot \frac{\Delta T}{\Delta t}, q_{net} - \rho_{ice} \cdot c_{ice} \cdot \Delta x \cdot \frac{\Delta T}{\Delta t}) & \text{if } T_{ice}^{i+1} \leq 0 \text{ and } \Delta M_F = 0 \\ (-\rho_{ice} \cdot c_{ice} \cdot \Delta x \cdot \frac{T_{ice}^i}{\Delta t}, q_{net} - q_L + \rho_{ice} \cdot c_{ice} \cdot \Delta x \cdot \frac{T_{ice}^i}{\Delta t}) & \text{if } T_{ice}^{i+1} > 0 \text{ and } \Delta M_F > 0 \\ (-\rho_{ice} \cdot c_{ice} \cdot \Delta x \cdot \frac{T_{ice}^i}{\Delta t}, q_{net} + \rho_{ice} \cdot c_{ice} \cdot \Delta x \cdot \frac{T_{ice}^i}{\Delta t}) & \text{if } T_{ice}^{i+1} > 0 \text{ and } \Delta M_F = 0 \end{cases} \quad (21)$$

**Table 1.** Free parameters in the model categorised as constant, uncertain and site parameters. Base value (B) and uncertainty (U) were taken from the literature. For assumptions (assum.), the uncertainty was chosen to be relatively large (5 %). For measurements (meas.), the uncertainty due to parallax errors is chosen to be (1 %).

Constant Parameters	Symbol	Value	Range	References
Van Karman constant	$\kappa$	0.4	n.a.	B: Cuffey and Paterson
Stefan Boltzmann constant	$\sigma$	$5.67 \cdot 10^{-8} W m^{-2} K^{-4}$	n.a.	B: Cuffey and Paterson
Air pressure at sea level	$p_{0,a}$	1013 hPa	n.a.	B: Mölg and Hardy
Density of water	$\rho_w$	1000 kg m <sup>-3</sup>	n.a.	B: Cuffey and Paterson
Density of ice	$\rho_{ice}$	917 kg m <sup>-3</sup>	n.a.	B: Cuffey and Paterson
Density of air	$\rho_a$	1.29 kg m <sup>-3</sup>	n.a.	B: Mölg and Hardy
Specific heat of water	$c_w$	4186 J kg <sup>-1</sup> °C <sup>-1</sup>	n.a.	B: Cuffey and Paterson
Specific heat of ice	$c_{ice}$	2097 J kg <sup>-1</sup> °C <sup>-1</sup>	n.a.	B: Cuffey and Paterson
Specific heat of air	$c_a$	1010 J kg <sup>-1</sup> °C <sup>-1</sup>	n.a.	B: Mölg and Hardy
Thermal conductivity of ice	$k_{ice}$	2.123 W m <sup>-1</sup> K <sup>-1</sup>	n.a.	B: Bonales et al.
Latent Heat of Sublimation	$L_s$	2848 kJ kg <sup>-1</sup>	n.a.	B: Cuffey and Paterson
Latent Heat of Evaporation	$L_e$	2514 kJ kg <sup>-1</sup>	n.a.	B: Cuffey and Paterson
Latent Heat of Fusion	$L_f$	334 kJ kg <sup>-1</sup>	n.a.	B: Cuffey and Paterson
Gravitational acceleration	$g$	9.81 m s <sup>-2</sup>	n.a.	B: Cuffey and Paterson
Uncertain Parameters				
Precipitation Temperature threshold	$T_{rain}$	1 °C	± 1 °C	B + U: Fujita and Ageta, Zhou et al.
Ice Emissivity	$\epsilon_{ice}$	0.95	± 5 %	B: Cuffey and Paterson; U: assum.
Ice Albedo	$\alpha_{ice}$	0.35	± 5 %	B: Cuffey and Paterson; U: assum.
Snow Albedo	$\alpha_{snow}$	0.85	± 5 %	B: Cuffey and Paterson; U: assum.
Albedo Decay Rate	$\tau$	10 days	[1, 22] days	B: Schmidt et al.; U: Oerlemans and Knap
Ice layer thickness	$\Delta x$	5 mm	[1, 10] mm	assum.
Site Parameters				
Fountain diameter	nozzle $dia_F$	5 mm	± 1 %	B: meas. ; U: assum.
Fountain Height	$h_F$	1.35 m	± 1 %	B: meas. ; U: assum.
Fountain temperature	water $T_{water}$	5 °C	[0, 9] °C	B: meas. ; U: meas.
AWS Height	$h_{AWS}$	3 m	± 1 %	B: meas. ; U: assum.

$$M_F + M_{ppt} + M_{dpt} = M_{ice} + M_{melt} + M_{vapour} + M_{drained} \quad (22)$$

where  $M_F$  denotes the cumulative water input;  $M_{ppt}$  is the cumulative precipitation and  $M_{dpt}$  is the cumulative accumulation through water vapour condensation or deposition;  $M_{ice}$  is the cumulative mass of ice;  $M_{melt}$  is the cumulative mass of melt water;  $M_{vapour}$  represents the cumulative water vapor loss by evaporation or sublimation and  $M_{drained}$  is the cumulative water that drains away.

Equation 22 can be rewritten using the mass balance change as:

$$\frac{\Delta M_F}{\Delta t} + \frac{\Delta M_{ppt}}{\Delta t} + \frac{\Delta M_{dpt}}{\Delta t} = \frac{\Delta M_{ice}}{\Delta t} + \frac{\Delta M_{melt}}{\Delta t} + \frac{\Delta M_{vapour}}{\Delta t} + \frac{\Delta M_{drained}}{\Delta t} \quad (23)$$

where  $\Delta M = M^i - M^{i-1}$ . Here  $\frac{\Delta M_F}{\Delta t} = d_F$  where  $d_F$  is the spray of the fountain measured in  $[kg\ s^{-1}]$ . Precipitation input is calculated as:

$$\frac{\Delta M_{ppt}}{\Delta t} = \begin{cases} \pi \cdot r_{ice}^2 \cdot \rho_w \cdot ppt & \text{if } T_a < T_{rain} \\ 0 & \text{if } T_a \geq T_{rain} \end{cases} \quad (24)$$

where  $\rho_w$  is the density of water ( $1000\ kg\ m^{-3}$ ),  $ppt$  is the measured precipitation rate in  $[m\ s^{-1}]$  and  $T_{rain}$  is the temperature threshold below which precipitation falls as snow. Here, snowfall events were identified using  $T_{rain}$  as  $1^\circ C$ . Snow mass input is calculated by assuming a uniform deposition over the entire circular footprint of the Icestupa.

The latent heat energy is used to estimate either the evaporation and condensation processes or sublimation and deposition processes. Deposition and sublimation involve phase change between vapour and ice whereas evaporation and condensation involve phase change between meltwater and ice. To differentiate between these two possibilities, we classify the time steps into humid or non-humid if the corresponding relative humidity value is above or below 60 % (Stigter et al., 2018). On humid time steps we assume condensation or evaporation to occur whereas on non-humid time steps deposition or sublimation can occur. Correspondingly, latent heat of evaporation ( $L_e$ ) is used for humid time steps and latent heat of sublimation ( $L_s$ ) is used for non-humid time steps. Water accumulation and vapour loss from the Icestupa surface is calculated as follows:

$$\left( \frac{\Delta M_{vapour}}{\Delta t}, \frac{\Delta M_{dpt}}{\Delta t} \right) = \begin{cases} (q_L \cdot A/L, 0) & \text{if } q_L < 0 \\ (0, -q_L \cdot A/L) & \text{if } q_L \geq 0 \end{cases} \quad (25)$$

$$\text{where } L = \begin{cases} L_e & \text{if } RH \geq 60 \\ L_s & \text{if } RH < 60 \end{cases}$$

Using the melt energy  $q_{melt}$ , we estimate the frozen and melted ice mass ( $\Delta M_{ice}$ ,  $\Delta M_{melt}$ ). Removing the contribution of precipitation and combining Eqn. 25 we are left with the contribution from the melt energy as follows:

**Table 2.** Summary of calculated mass balance components for the Schwarzsee experiment after the fountain spray was stopped on 15<sup>th</sup> February and at the end of the model run on 1<sup>st</sup> April.

	Mass Component	Fountain spray ends	Model ends
Input	$M_F$	18060 kg	18060 kg
	$M_{ppt}$	439 kg	463 kg
	$M_{dpt}$	14 kg	62 kg
Output	$M_{melt}$	166 kg	1392 kg
	$M_{ice}$	1158 kg	0 kg
	$M_{vapour}$	4 kg	8 kg
	$M_{drained}$	17184 kg	17184 kg

$$\left( \begin{array}{l} \left( \frac{\Delta M_{ice} - \Delta M_{ppt} - \Delta M_{dpt} + \Delta M_{vapour}}{\Delta t}, \frac{\Delta M_{melt}}{\Delta t} \right) \\ \left( \frac{\Delta M_{ice} - \Delta M_{ppt} - \Delta M_{dpt}}{\Delta t}, \frac{\Delta M_{melt} + \Delta M_{vapour}}{\Delta t} \right) \end{array} \right) = \left\{ \begin{array}{ll} \left( \frac{q_{melt} \cdot A}{L_f} \cdot (-1, 1) \right) & \text{if } q_{melt} \geq 0 \\ \left( \frac{q_{melt} \cdot A}{L_f} \cdot (-1, 0) \right) & \text{if } q_{melt} < 0 \text{ and } \frac{\Delta M_F}{\Delta t} \geq -q_{melt} \\ \left( \frac{\Delta M_F}{\Delta t}, 0 \right) & \text{if } q_{melt} < 0 \text{ and } 0 \leq \frac{\Delta M_F}{\Delta t} < -q_{melt} \end{array} \right. \quad (26)$$

Now, with all the other terms known in Eqn. 23, the water drained from the Icestupa can be expressed as:

$$\frac{\Delta M_{drained}}{\Delta t} = \frac{\Delta M_F + \Delta M_{ppt} + \Delta M_{dpt} - \Delta M_{ice} - \Delta M_{melt} - \Delta M_{vapour}}{\Delta t} \quad (27)$$

Considering AIR as water reservoirs, we can quantify their potential through the amount of water they store (storage quantity) and the length of time they store it (storage duration). Another means of comparing different Icestupas is through their water storage efficiency defined accordingly as:

$$\text{Storage Efficiency} = \frac{M_{melt}}{(M_F + M_{ppt} + M_{dpt})} \cdot 100 \quad (28)$$

## 4 MODEL RESULTS

The model was forced with meteorological data from 30<sup>th</sup> January to 1<sup>st</sup> April 2019 (Fig. 3) and various parameters (see Table 1) to calculate the mass and energy balance of the Icestupa.

### 4.1 Energy and mass balance calculation

Daily averages of some components of the energy balance are shown in Fig. 6 (a). On average during the experiment duration, the total energy flux from the atmosphere to the Icestupa are almost balanced. Net shortwave radiation ( $28 \text{ W m}^{-2}$ ), sensible ( $17 \text{ W m}^{-2}$ ) and latent heat flux ( $9 \text{ W m}^{-2}$ ) with a mostly



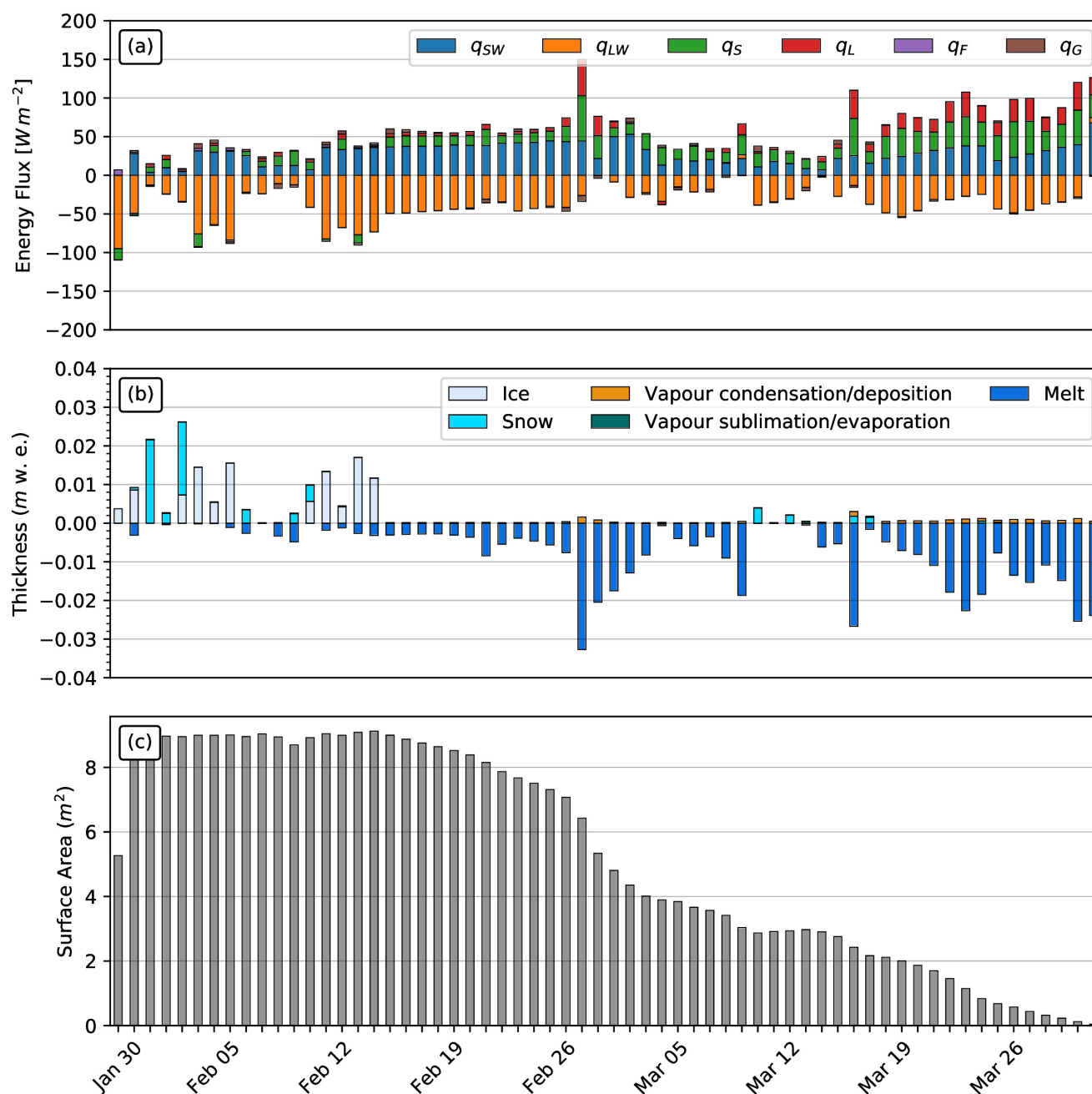


**Figure 6.** (a) Energy flux components, (b) mass flux components and (c) surface area of the Icestupa in daily time steps.  $q_{sw}$  is the net shortwave radiation;  $q_{LW}$  is the net longwave radiation;  $q_L$  and  $q_s$  are the turbulent latent and sensible heat fluxes.  $q_F$  represents the interactions of the ice-water boundary during fountain on time steps.  $q_G$  quantifies the heat conduction process between the Icestupa surface layer and the ice body.

positive flux towards the surface of the iclestupa are compensated by the net longwave radiation ( $-36 W m^{-2}$ ) and the melt energy ( $-19 W m^{-2}$ ). The contribution of other fluxes are negligible in comparison.

Net shortwave radiation is the main input to, and the most varying energy flux on the ice surface. Its variability is controlled by the surface albedo  $\alpha$  and the area fraction  $f_{cone}$  which therefore represent key variables in the energy balance (Fig. 7 (a)). Although global radiation flux reached a daily maximum value

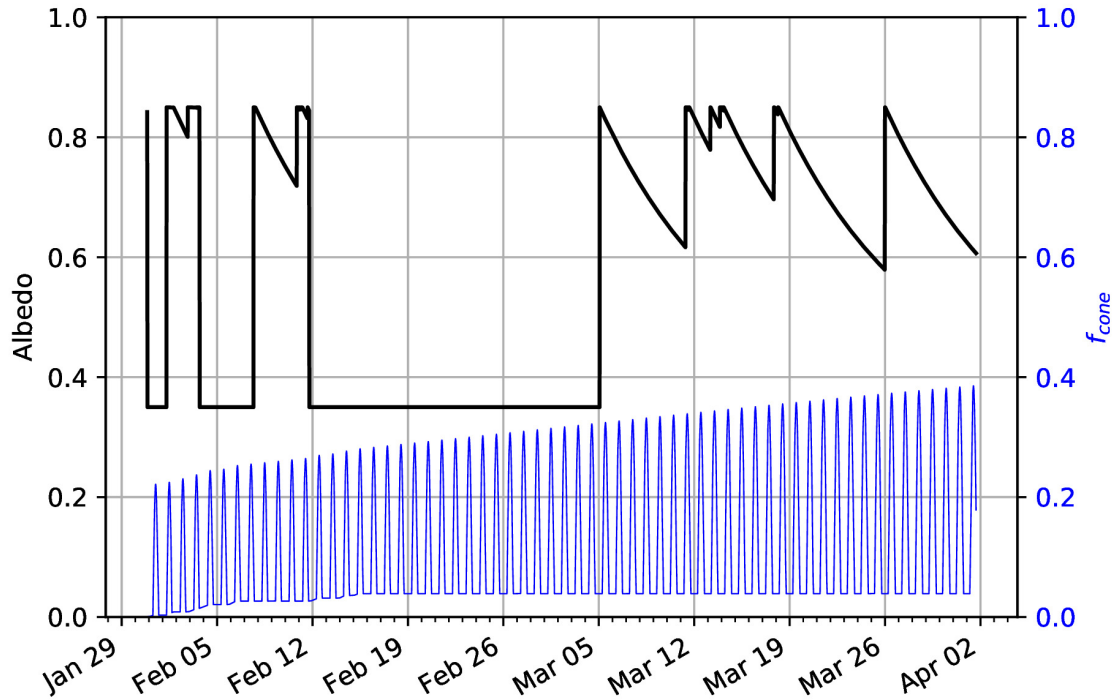


**Figure 7.** Some derived parameters of the model, namely, albedo and  $f_{cone}$  (a), Surface and bulk temperature (b). In (a), the black curve shows how snow and fountain-on events reset albedo between ice albedo and snow albedo. The decay of the snow albedo to ice albedo can also be observed. The blue curve shows how the solar radiation area fraction varied diurnally with variations in the solar elevation angle. In (b), the surface temperature (black curve) was forced to be  $0^{\circ}\text{C}$  during fountain activity. The corresponding bulk temperature is shown with the blue curve.

of  $304\text{ Wm}^{-2}$ ,  $q_{SW}$  only went up to  $68\text{ Wm}^{-2}$ . This is caused by the fact that only about 30 percent of the direct solar radiation influenced the Icestupa surface as shown by the area fraction  $f_{cone}$  in Fig. 7 (a). Snowfall is the atmospheric variable connected most closely and proportionally to albedo. Higher and/or more frequent snowfall thus decreases the energy available for melt due to the corresponding increase in  $\alpha$ .

$q_{LW}$  was predominantly negative indicating that this energy balance component drove the freezing of the ice structure. The incoming longwave radiation was strongly dependent on atmospheric emissivity which had a mean value of 0.77. Atmospheric emissivity in turn depended on the measured cloudiness factor. Daily values of  $q_{LW}$  ranged from  $-95$  to  $7\text{ Wm}^{-2}$ .  $q_{LW}$  and  $q_S$  were both proportional to the temperature gradient between the air and the Icestupa surface. Turbulent sensible heat flux  $q_S$  contributed mostly to the melt of the ice structure. Daily values of  $q_S$  ranged from  $-16$  to  $59\text{ Wm}^{-2}$ . Turbulent latent heat flux  $q_L$  was predominantly positive suggesting that it favoured deposition/condensation over evaporation/sublimation. Daily values of  $q_L$  ranged from  $-4$  to  $47\text{ Wm}^{-2}$ . Therefore, the Icestupa gained mass cumulatively from the atmosphere due to the deposition/condensation process. Fountain water heat flux  $q_F$  had a mean of zero as it was only nonzero during 1002 time steps or around 100 hours. Daily values of  $q_F$  ranged from  $0$  to  $7\text{ Wm}^{-2}$ . The contribution of heat flux by conduction  $q_G$  was minimal as it only varied between  $-7$  to  $7\text{ Wm}^{-2}$  with a mean of  $0\text{ Wm}^{-2}$ . The energy contributing to surface temperature changes ( $q_T$ ) was insignificant in comparison to the energy spent on freezing and melting ( $q_{melt}$ ). The resulting bulk temperature and the surface temperature are shown in Fig. 7 (b). For the total considered period,  $q_{LW}$  accounted for 28.3% of overall energy turnover. The energy turnover is calculated as the sum of energy

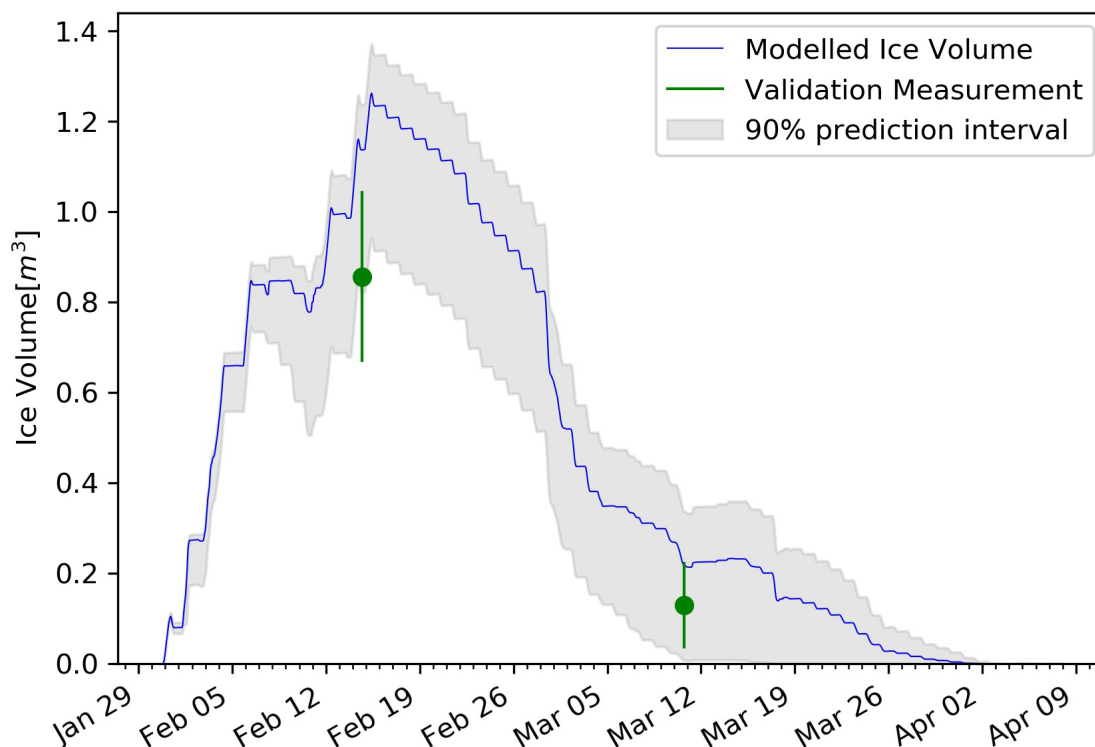


**Figure 8.** Modelled ice volume during the lifetime of the Schwarzsee Icestupa (blue curve). Green line segments indicate the first and second validation measurements. The prediction interval is based on the ice volume uncertainty caused by the most sensitive parameters, namely, temperature threshold below which precipitation falls as snow and the ice emissivity.

fluxes in absolute values.  $q_{SW}$  accounted for 21.7%, followed by  $q_{melt}$  (25.4%),  $q_S$  (14.6%),  $q_L$  (7.5%),  $q_G$  (1.8%),  $q_F$  (0.3%) and  $q_T$  (0.3%).

Fig. 6 (b) represents the mass fluxes associated with these energy exchanges expressed in  $m$  w.e. It shows the ice and meltwater formed due to  $q_{melt}$ , snow accumulated due to precipitation, water vapour deposition/condensation and sublimation/evaporation due to  $q_L$ . Growth rate ( $\frac{\Delta M_{ice}}{\Delta t}$ ) shows a strong correlation with net energy flux ( $r^2 = 0.44$ ) but poor correlation with Icestupa surface area ( $r^2 = 0.04$ ). This is because the variance in growth rate is mostly due to the variance in  $q_{net}$  as illustrated in Fig. 6. Since  $r_{ice}$  was initialised with the spray radius  $r_F$ , the surface area maintains a maximum initially until the energy flux becomes positive. This trend favours the positive over the negative thickness changes resulting in a steep increase and gradual melting of ice volume as can be seen in Fig. 8.

The total water used for the Icestupa development includes contributions from the fountain (97.2%), snowfall (2.5 %) and deposition/condensation (0.3 %) as shown in Table 2. The maximum ice mass during the whole measurement period was 1158 kg, which occurred after the last fountain run on Feb 16<sup>th</sup> in the morning. Therefore, in the case of Schwarzsee we used a water input of 18,584 kg, which is then resulting in a storage efficiency of only 7.5 %.

## 5 MODEL SENSITIVITY AND UNCERTAINTY ANALYSIS

The icedupa model can be regarded as a function  $f(x_1, x_2, \dots, x_n) = (y_1, y_2, \dots, y_m)$ , where  $(x_1, x_2, \dots, x_n)$  are the model parameters and  $(y_1, y_2, \dots, y_m)$  are the model outputs. The influence of each

parameter on the output variables of interest were quantified and the most important physical parameters for the subsequent uncertainty analysis were determined. The sensitivity of a parameter  $x_j$  is determined by keeping all other parameters  $x_i, i \neq j$  fixed at their baseline value and varying  $x_j$  within values that are physically plausible.

A sensitivity study on the parameters (listed in Table 1) was performed with the maximum ice volume as the target variable. All the parameters were assumed to be independent of each other with a uniform distribution. This assumption ignores the auto-correlation present among the parameters associated with the albedo parameterisation. The range of uncertain parameters were set based on available literature values or varied  $\pm 5\%$  from the base value if no such reference was available. The uncertainty of all the site parameters were caused due to parallax errors during manual measurement. This was quantified with a range of  $\pm 1\%$  from the base value. However, it must be kept in mind that, even though intended to be as objective as possible, the selection of a parameter range has a subjective part that influences the results and conclusions obtained in this analysis. The variation of the model outputs  $y_k$  is evaluated to quantify the local sensitivities  $s_{j,k}$  that are defined here as the 95% range of the simulated outputs.

To perform the uncertainty analysis, we included only parameters that influence the maximum ice volume by at least  $0.1m^3$ . All other parameters were fixed at their baseline value.

## 5.1 Model Simulations

The sensitivity and uncertainty analyses were performed systematically for each of the 10 parameters. In total, the sensitivity analysis required 120 simulations, and the uncertainty analysis a total of 32 simulations. Fig. 9 shows all the variance produced by these uncertain parameters in maximum ice volume calculation. It shows that  $\epsilon_{ice}$  and  $T_{rain}$  are the only parameters with a maximal sensitivity of more than  $0.1 m^3$  for the maximum ice volume estimate. Consequently, all other parameters were excluded from the subsequent uncertainty analysis.

The temperature threshold below which precipitation falls as snow ( $T_{rain}$ ) was found to be the most sensitive parameter. It is used in the model to reset the albedo to snow albedo and determine snow precipitation events. The lower  $T_{rain}$  parameter the higher the albedo (as the Icestupa surface has a lower albedo when ice-covered than when snow-covered). The variation of  $T_{rain}$  by 5% caused maximum ice volume variation of  $1.2 \pm 0.2m^3$ .

Ice emissivity was also found to be a sensitive parameter. The higher the ice emissivity the larger the maximum ice volume as the emitted longwave radiation increases with ice emissivity. Variation of  $\epsilon_{ice}$  by 5% caused a maximum ice volume range from  $1.3 \pm 0.1m^3$ .

## 6 DISCUSSION

### 6.1 Model validation quality

We first evaluate the model against the validation measurements at the Schwarzsee site. The uncalibrated model is able to capture both the freezing and the melting process sufficiently well as the modelled ice volume lies within the uncertainty of both validation measurements. Furthermore, the validation measurements fit well within the estimated model uncertainty. However, since this validation is based on only two points, it does limit the confidence in the model results. Moreover, the model seems to overestimate the ice volume at both validation points. This could be due to the underestimation of the surface area which underestimates the melt rates (absolute growth rate when  $\frac{\Delta M_F}{\Delta t} < 0$ ) and the freeze rates (absolute growth rate when  $\frac{\Delta M_F}{\Delta t} > 0$ ). However, as the fountain was mostly inactive during the study period, the underestimation of surface area disproportionately undervalues the melt rates over the freeze

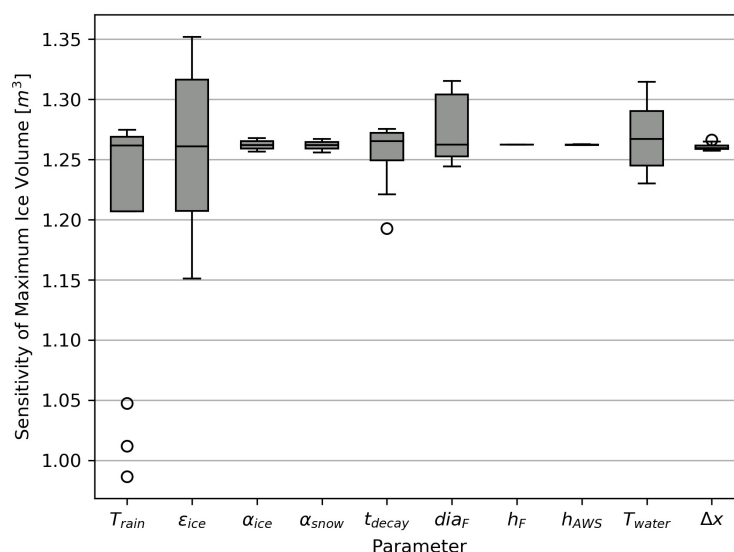


**Figure 9.** Sensitivities of maximum ice volume to all the uncertain and site parameters used in the model (Table 1). Outliers in the bar plot are shown as 'o'.

rates. One major cause of this underestimation was the conical shape assumption, as in reality, the Icestupa shape ranged between a cone and a cylinder (Fig. 2). Another cause was the surface irregularities that were observed due to uneven exposure to direct solar radiation and fountain droplets. The sensitivity of the model results to these errors was further amplified due to the relatively small volume of the Schwarzsee Icestupa. In summary, more validation measurements on a more voluminous Icestupa would have increased confidence on the model results.

## 6.2 Important assumptions

In the sensitivity and uncertainty analysis presented above, we did not account for several general assumptions and parametrisation choices that may cause model errors. Some assumptions and their potential to cause errors are discussed below.

- **Turbulent Sensible and Latent Heat Fluxes:** The method used to calculate the turbulent heat fluxes by Garratt (1992) assumes that the turbulent heat fluxes are acting over a uniform planar surface to determine the roughness length. Since our application is on a conical surface,  $z_{ice}$  has no real physical significance.
- **Droplet flight time loss:** Water losses during the flight time of fountain droplets were neglected making all the fountain spray available for freezing. For the Schwarzsee experiment, inclusion of this parameter does not influence results since it is already accounted for in the drained water discharge rate which was at least  $3 \text{ l min}^{-1}$ .
- **Nucleation of droplets:** Corresponding to droplet flight time, ice/snow formation is also possible before surface contact if nucleation occurs during flight time. For the Schwarzsee experiment, this process will further increase the freeze rate and hence the storage efficiency. This process is neglected for model simplicity.

## 6.3 Schwarzsee vs Ladakh Icestupa

Icestupa 2014/15 in Ladakh had a storage quantity of around 2 million litres of water and a storage duration of around 5 months (see Appendix 8.1). In contrast, the presented Schwarzsee Icestupa has only a

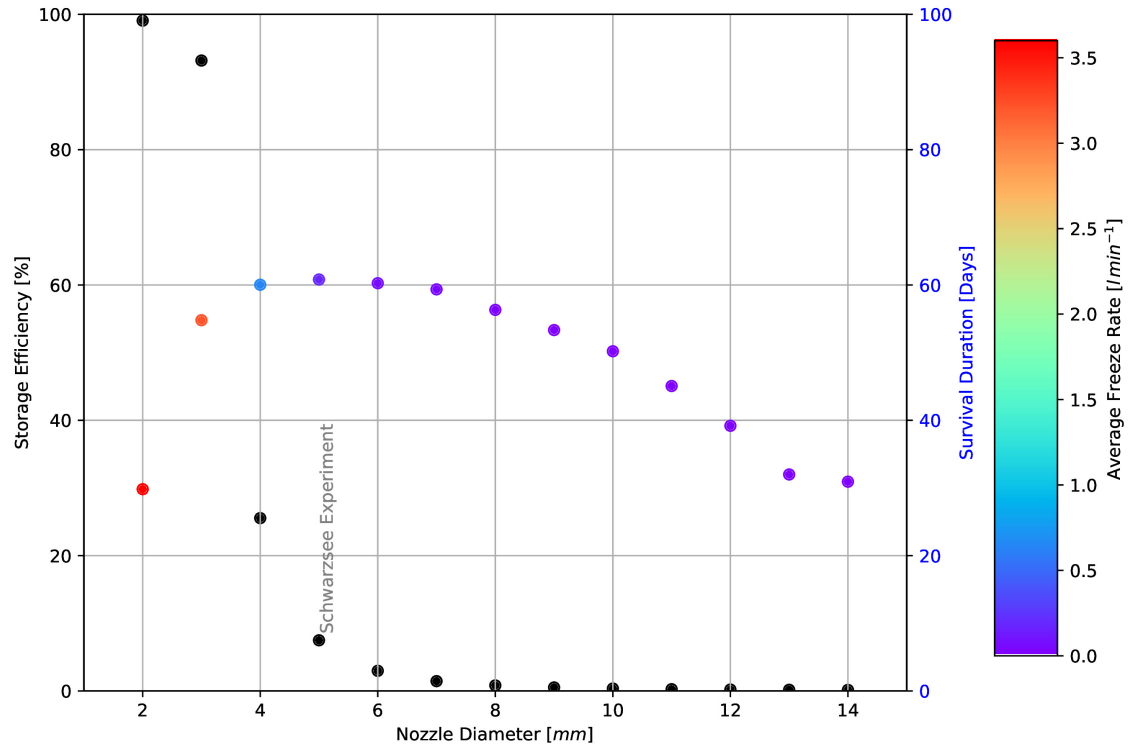


**Figure 10.** Variation in storage efficiency (black dots) and storage duration (coloured dots) with changes in fountain nozzle's nozzle diameter. The dot colours represent average freeze rate based on the color bar.

storage quantity of 1392 *litres* and a storage duration of 61 days, which is not very representative to fully capture the seasonal Icestupa dynamics. However, this is the only Icestupa dataset available to this date. We believe that the model is capable to capture at least the most important processes involved in the build up and melt of a simplified Icestupa assuming a cone shaped structure.

Table 2 clearly shows that for our Schwarzsee experiment most of the input water (92 %) simply drained away. This high water loss through drainage is due to the fact that the average spray rate of the fountain ( $(\frac{\Delta M_F}{\Delta t})_{mean} = 3.6 \text{ l min}^{-1}$ ) far exceeded the max Icestupa growth rate ( $(\frac{\Delta M_{ice}}{\Delta t})_{max} = 1 \text{ l min}^{-1} \text{ (w.e.)}$ ).

In the city of Leh, Ladakh at an altitude of 3500 *m* a.s.l. the air temperature shows values down to 27.9 °C in winter (Chevuturi et al., 2018) whereas Schwarzsee had a minimum temperature of just -11.6 °C during the study period. Moreover, subzero temperatures were only reached for 7 nights of fountain operation at the Schwarzsee site compared to the 43 nights of fountain operation possible in Ladakh (see Appendix 8.1). Thus, the Icestupa growth rate is expected to be much higher in Ladakh. However, water spray rates in Ladakh are also much higher (around 210  $\text{l min}^{-1}$ ). So the water losses in Ladakh could also be caused due to excessive fountain spray.

#### 6.4 Icestupa construction decisions

There are several decisions one has to take when constructing Icestupas. These can be broadly divided into two types of decisions, namely fountain and location decisions. Both the meteorological conditions of the location and the surface area produced by the fountain significantly influence the observed growth rate. Since our validation is restricted to just one location, we restrict our discussion to the optimization possibilities of Icestupa constructions through fountain decisions.



Assuming a constant spray for the fountain, we can divide the fountain decisions into fountain state (on/off) and type (height and nozzle diameter). From an energy balance point of view, the fountain should be switched on for all time intervals when  $q_{net} < 0$ . However, in our experiment, the fountain state decision was set based on whether the ambient temperature was above or below a critical temperature of  $-5^{\circ}\text{C}$ . Ambient temperature can serve as an indicator of  $q_{net}$  as it was correlated ( $r^2 = 0.53$ ). However,  $q_{net}$  was found to be negative already at a critical temperature of  $-1^{\circ}\text{C}$ . Therefore, using air temperature to determine when the fountain should be switched on is justified but a higher critical temperature could have been used in the case of the Schwarzsee Icestupa.

The fountain type used can be characterised by the physical structure of the fountain, namely its height and nozzle diameter. Maintaining the same spray rate and height, one can optimize the Icestupa development by identifying the minimum nozzle diameter that yields the maximum storage efficiency.

Fig. 10 shows reducing the nozzle diameter to 3 mm increases storage efficiency up to 93 % without compromising much on storage duration. The corresponding storage quantity of the 3 mm nozzle diameter was more than 20 times higher than the 5 mm fountain used in our experiment. This is because the spray radius  $r_F$  of the 3 mm fountain was much higher at 8.5 m compared to the 1.7 m spray radius of the 5 mm fountain (see Appendix Section 8.2). Here, we define growth rate as freeze rate when fountain is active and melt rate otherwise. So this higher spray radius both, increases the freeze rate and increases the melt rate since they are both directly proportional to the surface area. However, since the freeze rate cannot increase beyond a spray rate of  $3.6 \text{ l min}^{-1}$  (except during precipitation or deposition/condensation events), an optimum spray radius or nozzle diameter exists, beyond which storage duration suffers due to a disproportionate increase in melt rate compared to the freeze rate. So even though 3 mm nozzle diameter had a much higher storage quantity than the 5 mm nozzle, its storage duration was around 6 days lesser than the 5 mm nozzle. One physical cause of this effect is the different shapes of both the ice structures. A flat sheet of ice (effectively a cone with a high spray radius) with higher mass might have a storage duration shorter than a conical ice structure. As the spray radius decreases with increasing nozzle diameter, the ice structure's average slope increases and so the 5 mm nozzle's ice structure is "more" conical than the 3 mm ice structure. Fig. 10 shows that a nozzle diameter of 3 mm has an average freeze rate ( $3.2 \text{ l min}^{-1} \text{ w.e.}$ ) which is large enough to increase the storage efficiency and small enough to not reduce the storage duration of the Icestupa significantly.

## 7 CONCLUSIONS

We have outlined a methodology for estimating ice, liquid water, water vapour and drained quantities produced during the construction of an Icestupa using measurements of fountain spray rate, air temperature, radiation, humidity, pressure, wind and cloudiness at the Schwarzsee study site. The comparison with validation measurements at two different dates during the experiment led to satisfying results. However, the validation quality still could have been improved by having performed more such measurements.

According to the model, the Schwarzsee Icestupa achieved a storage quantity of 1392 litres of water with a storage duration of 61 days. However, the corresponding storage efficiency was very low with only 7.5 % for a water input of 18,584 litres. These estimates were most sensitive to the temperature threshold that determined precipitation phase and ice emissivity parameters which created an uncertainty of  $1.2 \pm 0.3 \text{ m}^3$  in the maximum ice volume calculated. This is to be expected as net longwave radiation and net shortwave radiation together accounted for around 50 % of the overall energy turnover.

Although the location, storage quantity and duration of our experimental Schwarzsee Icestupa are not representative of the much larger Icestupas of Ladakh, the model results do support the hypothesis that

there could be considerable water loss during the formation of Icestupas particularly due to excessive fountain spray. Using model calculations, it was shown that a decreased fountain nozzle diameter of 3 mm can increase the storage efficiency drastically. This is because a change in the fountain nozzle diameter causes an effective change of the ice surface area over which the net energy flux can act. This result has relevance on the future design of Icestupa fountains. However, care has to be taken as our model is currently only validated by one experiment at the Schwarzsee site. Further experiments at different locations with different fountains are required to better understand the influence of construction decisions on the results.

## 8 APPENDIX

### 8.1 Ladakh Icestupa 2014/15

A 20 m tall Icestupa (Wangchuk, 2015c) was built in Phyang village, Ladakh at an altitude of 3500 m a.s.l. Assuming a conical shape with a diameter of 20 m, the corresponding volume of this Icestupa becomes 2093 m<sup>3</sup> or 1,919,587 litres w.e. The fountain sprayed water at a rate of 3.5 l s<sup>-1</sup> (Wangchuk, 2015e) from 21<sup>st</sup> January (Wangchuk, 2015a) to at least until 5<sup>th</sup> March 2015 (Wangchuk, 2015b) (around 43 nights). Assuming fountain spray was active for 8 hours each night, we estimate water consumption to be around 4,334,400 litres. So just during construction/freezing period of the Icestupa, roughly 56 % of the water provided was wasted. The actual water loss is bound to be much higher due to further vapour losses during the melting period. This Icestupa completely melted away on 6<sup>th</sup> July 2015 (Wangchuk, 2015d). Therefore, the storage duration was 166 days or roughly 5 months.

### 8.2 Mean Spray Radius $r_F$

The fountain spray radius is determined by modelling the projectile motion of the water droplets. Using mass conservation the droplet speed  $v_F$  can be determined from the spray rate  $d_F$  and the diameter  $dia_F$  of the nozzle as follows:

$$v_F = \frac{d_F}{\pi \cdot dia_F^2 / 4} \quad (29)$$

Afterwards, we assume that the water droplets move with an air friction free projectile motion from the fountain nozzle with a height  $h_F$  to the ice/ground surface. The resulting spray radius  $r_F$  was then determined from the projectile motion equation as follows:

$$r_F = \frac{v_F \cdot \cos\theta_F (v_F \cdot \sin\theta_F + \sqrt{(v_F \cdot \sin\theta_F)^2 + 2 \cdot g \cdot h_F})}{g} \quad (30)$$

where  $g = 9.8ms^{-2}$  is the acceleration due to gravity and  $\theta_F = 45^\circ$  is the angle of launch.

## CONFLICT OF INTEREST STATEMENT

The authors declare that the research was conducted in the absence of any commercial or financial relationships that could be construed as a potential conflict of interest.

## AUTHOR CONTRIBUTIONS

SB wrote the initial version of the manuscript. MH, ML, SW, JO, and FK commented on the initial manuscript and helped improve it. SB developed the methodology with inputs from MH. SB performed the analysis with support from MH and ML. SB and MH participated in the fieldwork.

## FUNDING

This work was supported and funded by the University of Fribourg and by the Swiss Government Excellence Scholarship (Suryanarayanan Balasubramanian).

## ACKNOWLEDGMENTS

We thank Mr. Adolf Kaeser and Mr. Flavio Catillaz at Eispalast Schwarzsee for their active participation in the fieldwork. We would also like to thank Digmesa AG for subsidising their flowmeter used in the experiment. We would particularly like to thank the editor Prof. Thomas Schuler who gave us important inputs to improve the paper and we thank also Prof. Christian Hauck and Prof. Nanna B. Karlsson for valuable suggestions that improved the manuscript.

## DATA AVAILABILITY STATEMENT

The data and code used to produce results and figures will be published at a later stage and can, until then, be obtained from the authors upon request.

## REFERENCES

- Apel, H., Abdykerimova, Z., Agalhanova, M., Baimaganbetov, A., Gavrilenko, N., Gerlitz, L., et al. (2018). Statistical forecast of seasonal discharge in central asia using observational records: development of a generic linear modelling tool for operational water resource management. *Hydrology and Earth System Sciences* 22, 2225–2254. doi:10.5194/hess-22-2225-2018
- Bonales, L. J., Rodriguez, A. C., and Sanz, P. D. (2017). Thermal conductivity of ice prepared under different conditions. *International Journal of Food Properties* 20, 610–619. doi:10.1080/10942912.2017.1306551
- Brutsaert, W. (1975). On a derivable formula for long-wave radiation from clear skies. *Water Resources Research* 11, 742–744. doi:10.1029/WR011i005p00742
- Brutsaert, W. (1982). *Evaporation into the Atmosphere. Theory, History and Application* (Kluwer Academic Publishers)
- Buytaert, W., Moulds, S., Acosta, L., Bievre, B. D., Olmos, C., Villacis, M., et al. (2017). Glacial melt content of water use in the tropical andes. *Environmental Research Letters* 12, 114014. doi:10.1088/1748-9326/aa926c
- Chen, Y., Li, W., Deng, H., Fang, G., and Li, Z. (2016). Changes in central asia's water tower: Past, present and future. *Nature* doi:10.1088/1748-9326/aa926c
- Chevuturi, A., Dimri, A. P., and Thayyen, R. J. (2018). Climate change over leh (ladakh), india. *Theoretical and Applied Climatology* 131, 531–545. doi:10.1007/s00704-016-1989-1
- [Dataset] Copernicus Climate Change Service (C3S) (2017). Era5: Fifth generation of ecmwf atmospheric reanalyses of the global climate
- Cuffey, K. M. and Paterson, W. S. B. (2010). *The Physics Of Glaciers* (Elsevier)
- Fujita, K. and Ageta, Y. (2000). Effect of summer accumulation on glacier mass balance on the tibetan plateau revealed by mass-balance model. *Journal of Glaciology* 46, 244–252. doi:10.3189/172756500781832945
- Garratt, J. R. (1992). *The Atmospheric Boundary Layer* (Cambridge University Press)
- Grossman, D. (2015). As himalayan glaciers melt, two towns face the fallout
- Hock, R., Rasul, G., Adler, C., Cáceres, B., Gruber, S., Hirabayashi, Y., et al. (2019). 2019: High mountain areas. *IPCC Special Report on the Ocean and Cryosphere in a Changing Climate* [H.-O. Pörtner, D.C.

- Roberts, V. Masson-Delmotte, P. Zhai, M. Tignor, E. Poloczanska, K. Mintenbeck, A. Alegria, M. Nicolai, A. Okem, J. Petzold, B. Rama, N.M. Weyer (eds.)]
- Hoelzle, M., Barandun, M., Bolch, T., Fiddes, J., Gafurov, A., Muccione, V., et al. (2019). *The status and role of the alpine cryosphere in Central Asia*. doi:10.4324/9780429436475-8
- [Dataset] IDAWEB (2019). Meteoswiss, federal office of meteorology and climatology
- Immerzeel, W. W., Lutz, A. F., Andrade, M., Bahl, A., Biemans, H., Bolch, T., et al. (2019). Importance and vulnerability of the world's water towers. *Nature* 577, 364 – 369. doi:10.1038/s41586-019-1822-y
- Meteoblue (2020). Climate schwarzsee
- Mölg, T. and Hardy, D. R. (2004). Ablation and associated energy balance of a horizontal glacier surface on kilimanjaro. *J. Geophys. Res.-Atmos.* 109, 1–13. doi:10.1029/2003JD004338
- Nüsser, M., Dame, J., Kraus, B., Baghel, R., and Schmidt, S. (2019a). Socio-hydrology of artificial glaciers in ladakh, india: assessing adaptive strategies in a changing cryosphere. *Regional Environmental Change* doi:10.1007/s10113-018-1372-0
- Nüsser, M., Dame, J., Parveen, S., Kraus, B., Baghel, R., and Schmidt, S. (2019b). Cryosphere-Fed Irrigation Networks in the Northwestern Himalaya: Precarious Livelihoods and Adaptation Strategies Under the Impact of Climate Change. *Mountain Research and Development* 39. doi:10.1659/MRD-JOURNAL-D-18-00072.1
- Oerlemans, J. and Knap, W. H. (1998). A 1 year record of global radiation and albedo in the ablation zone of morteratschgletscher, switzerland. *Journal of Glaciology* 44, 231–238. doi:10.3189/S0022143000002574
- Schmidt, L. S., Aðalgeirsdóttir, G., Guðmundsson, S., Langen, P. L., Pálsson, F., Mottram, R., et al. (2017). The importance of accurate glacier albedo for estimates of surface mass balance on vatnajökull: evaluating the surface energy budget in a regional climate model with automatic weather station observations. *The Cryosphere* 11, 1665–1684. doi:10.5194/tc-11-1665-2017
- Stigter, E. E., Litt, M., Steiner, J. F., Bonekamp, P. N. J., Shea, J. M., Bierkens, M. F. P., et al. (2018). The importance of snow sublimation on a himalayan glacier. *Frontiers in Earth Science* 6, 108. doi:10.3389/feart.2018.00108
- Unger-Shayesteh, K., Vorogushyn, S., Farinotti, D., Gafurov, A., Duethmann, D., Mandychhev, A., et al. (2013). What do we know about past changes in the water cycle of central asian headwaters? a review. *Global and Planetary Change* 110, 4 – 25. doi:10.1016/j.gloplacha.2013.02.004. Water in Central Asia – Perspectives under global change
- Wangchuk, S. (2014). Ice stupa artificial glaciers of ladakh
- Wangchuk, S. (2015a). The good news at ice stupa 24th january 2015
- Wangchuk, S. (2015b). Ice stupa artificial glacier inaugurated 5th of march 2015
- Wangchuk, S. (2015c). Ice stupa surpasses guinness world record
- Wangchuk, S. (2015d). Ice stupa way of celebrating a special day
- Wangchuk, S. (2015e). World water day at ice stupa
- WMO (2018). *Guide to Instruments and Methods of Observation* (World Meteorological Organization ; 2018 (2018 Edition))
- Woolf, H. M. (1968). *On the Computation of Solar Elevation Angles and the determination of sunrise and sunset times* (National Aeronautics and Space Administration)
- Zhou, S., ShiQiao nd Kang, Gao, T., and Zhang, G. (2010). Response of zhadang glacier runoff in nam co basin, tibet, to changes in air temperature and precipitation form. *Chinese Science Bulletin* 55, 2103–2110. doi:10.1007/s11434-010-3290-5